Carbon Dioxide Sensor Substrate for Surface-mounted Packaging

Hyeuk-Jin Han, Tae Wan Kim, Kwang-Min Park, and Chong-Ook Park[+]

Abstract

Solid state electrochemical and chemo-resistive gas sensors have been used widely but can operate only under high temperature. For reducing the power consumption and optimizing the structure of the substrate of these sensors, we conducted device and circuit simulations using the COMSOL Multiphysics simulator. For assessing the effective types of substrate and heat isolation, we conducted three-dimensional thermal simulations in two separate parts; (a) by changing the shape of the contacting holes and (b) punching additional holes on the substrate. Thus, it was possible to achieve high temperature in the sensor end of the substrate while maintaining low power consumption, and temperature in the circuit.

Keywords: Simulation, Sensor substrate, Heat transfer effect

1. INTRODUCTION

Solid state electrochemical and chemo-resistive gas sensors have been used extensively in various gas sensing applications because of their advantages such as small size, durability and cheap price [1,2]. However, these devices have to be operated at elevated temperatures, in the ranges 300-350°C and 400-500°C in the case of resistive and solid electrolyte sensors, respectively.

Therefore, a localized heating scheme at or near the sensing element is needed for ensuring the thermal isolation and preventing heat conduction through the paths connecting the electronic circuits that are mainly formed on the Printed Circuit Board (PCB). The air-floating package is the most well-known and popular method for meeting this requirement. In such devices, the low thermal conductivity of air (0.024 W/m·K compared to 35 W/m·K for Al_2O_3) serves to maximize the localization of heat [3].

However, the air-floating structure causes large thermal loss through the connection lines to the circuit. For example, using an Au connection wire of 25 μm diameter results in incremental power dissipation of up to 30 mW per line at an operating temperature of 400°C. It also presents other drawbacks, such as

Materials science and Engineering, Korea Advanced Institute of Science and Technology (KAIST), 291 Daehak-ro, Yuseong-gu, Daejeon, 305-338, Korea
[+]Corresponding author: copark@kaist.ac.kr

frequent failures resulting from mechanical shock or creep of metal wires, incompatibility with electronic circuits, low productivity and large size [4].

Therefore, a better design that offers durability and compatibility with electronic packaging, while still retarding the propagation of thermal energy from the heated sensor to the main circuit board is required. High thermal energy transfer causes malfunction of the circuit and high overall power consumption.

To overcome the abovementioned disadvantages, heat must be distributed asymmetrically near the sensor and the temperature of the electronic connection pin should remain lower than 70°C. This study seeks to design an optimized substrate structure through numerical simulation of thermal distribution in various substrate geometries. The COMSOL Multi-physics program was used for simulating the temperature and power consumption.

2. EXPERIMENTAL

2.1 Preparation of sensor and sensor substrate

Two shapes of sensor-sitting sites with rectangular and circular holes were studied for solid electrolyte electrochemical sensors that are normally operated over 400°C, as shown in Fig. 1. The sensor was designed to be placed on the top of the hole to achieve an electrical contact between its metallic pads and the connecting lines in the substrate, as illustrated in the inset of Fig. 1. Substrate materials were assumed to be Al_2O_3, and Low Temperature Co-fired Ceramics (LTCC), having thermal conductivities of 35 and 3.3 W/m·K, respectively.
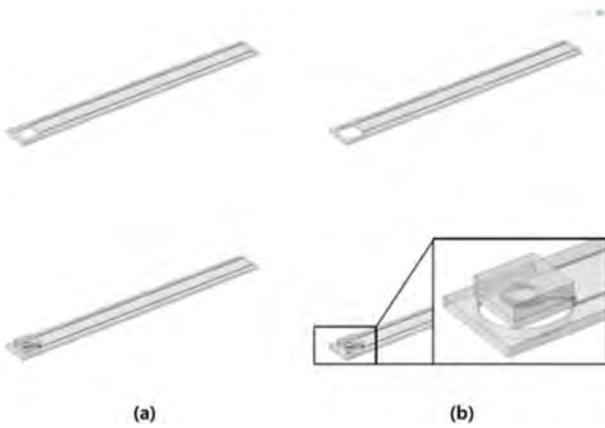
Fig. 1. Substrate design for simulation with (bottom) and without (top) sensor: (a) substrate with rectangular hole and (b) substrate with circular hole.
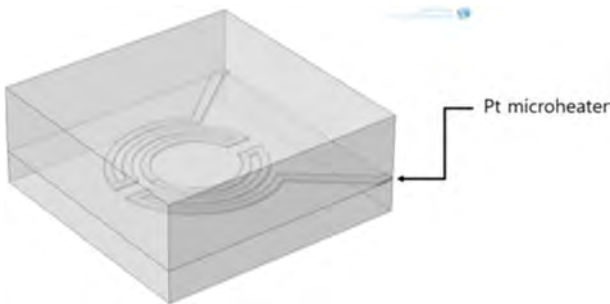

Fig. 2. Structure of 3D CO_2 sensor with microheater.

The size of the sensor was fixed at 3×3 mm and its thickness at 1.2 mm which correspond to a rather small sized sensor used in the field. A Pt micro heater was positioned in the sensor. The overall structure (shown in Fig. 2) was fabricated using the tape-casting method.

2.1.1 Three-dimensional (3D) electro thermal device simulations

The steady-state temperature distribution along the substrate resulting from joule heating in the sensor was studied using a commercial 3D finite element analysis program (COMSOL Multiphysics 4.2a). The power consumption was also calculated at the steady-current state using the value of the constant applied voltage. Here, conduction along the substrate, radiation to the air and natural convection over the sensor and substrate were considered as the elements of heat loss.

The mathematical expression for heat transfer by conduction is given by

$$\rho C \frac{\partial T}{\partial t} = Q + \nabla \cdot (k \nabla T) \tag{1}$$
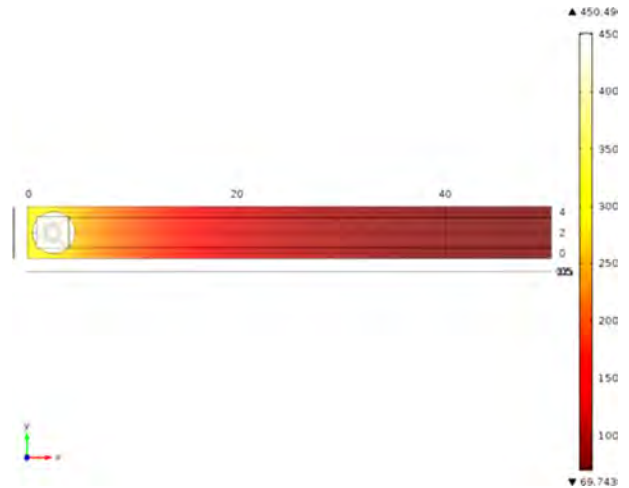

Fig. 3. Simulated result for sensor on Al_2O_3 substrate.

where ρ is the density of materials, T, C, k, t represent the density of materials, temperature, heat capacity, thermal conductivity, and time, respectively, and Q corresponds to the various heat sources and sinks. For example, the heater represents the heat source and radiation and convection loss represent heat sinks in Eq. (1). The heat generated by joule heating is given by Eq. (2).

$$Q = \frac{1}{\sigma} |J|^2 = \frac{I^2 R}{unit\ volume} \tag{2}$$

where σ and J represent the electric conductivity and current density, respectively.

The heat losses from radiation are given by Eq.

$$-n \cdot (-k \nabla T) = \varepsilon \sigma (T_{amb}^4 - T^4) \tag{3}$$

where n, σ, T, and ε represent the normal vector of the surface, Stefan–Boltzmann constant, temperature, and surface emissivity, respectively. The heat losses from convection are given by Eq. (4).

$$-n \cdot (-k \nabla T) = h(T_{amb} - T) \tag{4}$$

where h and T represent the convective heat transfer coefficient and temperature of the system, respectively, and T_{amb} is the temperature of air along the surface of the substrate, which is given by Eq. (5).

$$T_{amb} = 293.15K \tag{5}$$

The typical parameters for the substrate structure and physical constants used in the simulations are listed in Tables 1 and 2, respectively.

In this study, Equation (1) was solved by means of finite element analysis using COMSOL 4.2a. For example, in the illustration of temperature distribution in the substrate (shown in

Table 1. Geometrical and process parameters used in simulations

Description	Value
Sensor thickness	1.2 mm
Substrate thickness	0.5 mm
Substrate area	5×50 mm
Sensor area	3×3 mm

Table 2. Physical properties of materials used in simulations

Material	Thermal conductivity (W/m·K)	Specific heat (J/kg·K)	Density (kg/m^3)
Alumina	35.000	730	3950.0
Platinum	71.600	730	21450.0
Air	0.024	1030	1.1

Fig. 3), for an applied voltage bias, E = 6.50 V, which corresponds to 2.95 W of dissipated power. This results in a sensor temperature of 450°C. This calculation explicitly considered the abovementioned assumptions.

3. RESULTS AND DISCUSSIONS

3.1 Results of modeling and simulation

We performed device and circuit simulations using the COMSOL Multiphysics simulator. To assess the effective types of substrate and heat isolation, 3D thermal simulations were conducted in two separate parts: first, by changing the shape of the contacting hole and second, by punching additional holes in the substrate. The combinations of these features are regarded to be very effective in reducing heat conduction losses. Therefore, it was possible to achieve high temperatures in the sensor-end of the substrate while maintaining low power consumption and temperature in the circuit.

3.1.1 Type of contact shape

In the square-type model (shown in Fig. 4a), when the contact area was decreased to 0.03 from 0.12 mm^2, the power consumption reduced from 4.25 to 4.21 W. With decrease in the contact area, the temperature was found to decrease slightly, to 84.39 from 84.81°C. In the circle-type model (shown in Fig. 4b), however, the power consumption reduced from 3.38 to 2.95 W when the contact area was decreased to 0.03 from 0.12 mm^2, and the temperature fell from 75.2 to 69.7°C.

The above trend reveals that even with the same contact area, there is a large difference in the consumed power and lowest
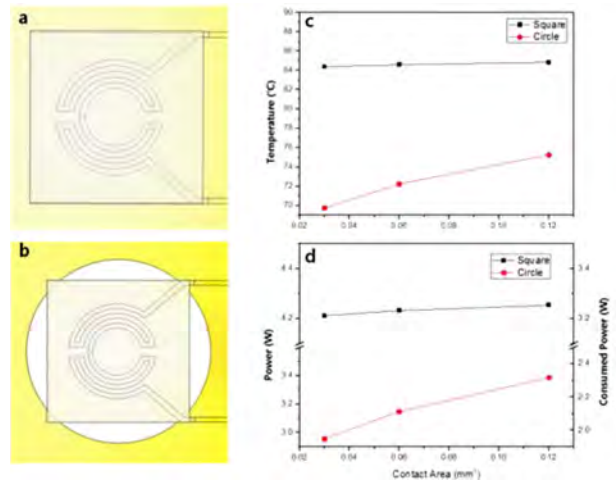

Fig. 4. Effects in different models: (a) Square-type model, (b) Circle-type model, (c) Temperature difference across models upon changing contact area, (d) Power difference between models upon changing contact area.

temperature achieved, among models with two types of contact shapes. There was a difference of approximately 15°C and over 1 W in the temperature and consumed power, respectively, between the two models. The results are summarized in Figs. 4c and 4d. In Fig. 4c, the right-side value shows the consumed power for the substrate without considering the power consumed by the sensor.

3.1.2 Sub-hole area effect

Next, we investigated the effect of additional holes made to the part of the substrate that was not in contact with the sensor. In this simulation, a circle-type substrate was used because it was observed to be more efficient based on the results with the types of contact shapes.

In this experiment, the areas of the holes were increased, and the temperature and consumed power were simulated in each case for contact areas of 0.03, 0.06, and 0.12 mm^2 (radius 2.035, 2.000, and 1.950 mm, respectively). After fixing the contact area, square-type holes were punched into the substrate of size 2×2 mm, with a distance of 0.5 mm between each hole. The increased areas of the holes are shown in Fig. 5a.

In the case of contact area of 0.12 mm^2 (radius 1.950 mm), the power reduced to 3.23 from 3.38 W with the increase in hole area to 20 mm^2, and the end-of-the-plate temperature decreased from 75.23 to 66.13°C. In similar cases of contact areas 0.06 and 0.03 mm^2, the consumed power decreased from 3.14 to 3.02 W and 2.95 to 2.85 W, respectively. The temperature also reduced from 72.25 to 63.85°C and 69.74 to 61.88°C, respectively.

When the area of the holes was 20 mm^2, there was a difference
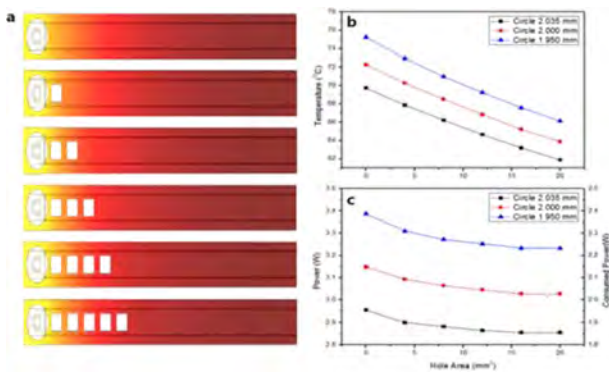
Fig. 5. Effects by hole area: (a) Process of changing hole area, (b) Temperature difference across contact area models upon changing hole area, (c) Power difference across contact area models upon changing hole area.
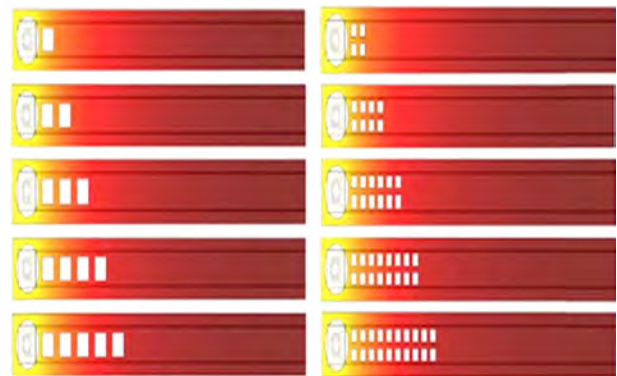

Fig. 6. Comparison of difference in process for changing hole area (for large and small holes)

Fig. 7. Effects by hole sizes in case of same hole area: (a) Temperature difference based on hole size, (b) Power difference based on contact hole size

in temperature and consumed power of approximately 5°C and 0.4 W, respectively, for a change in radius from 1.950 to 2.035 mm. The results are summarized in Figs. 5b and 5c. From the results, it can be concluded that increasing the area of the holes and decreasing the contact area produces significant power saving and temperature reducing effects.

3.1.3 Sub-hole size effect

Finally, we attempted to observe how the consumed power and temperature changed because of the differences in the sizes of holes for the same hole area. In this experiment, the contact area was fixed at 0.03 mm² for the models and the hole size was changed in two ways: either by maintaining a big or small hole. The sizes of the big and small holes were fixed at 2×2 mm and 1×1 mm, respectively. The process is shown in Fig. 6.

When the area of the holes was increased, the temperature decreased from 69.74 to 61.88°C and from 69.74 to 59.18°C for large and small holes, respectively, as shown in Fig. 7a. However, when the area of the holes was increased, the consumed power did not decrease significantly in the case of small holes compared to that in the case of large holes, which witnessed a reduction in power consumption. The difference in power consumption across the cases with small and large holes was approximately 0.1 W, as shown in Fig. 7b.

This result indicates that small holes do not affect the power consumption. Comparing the differences between the cases with large and small holes (shown in Fig. 7b), it can be seen that small holes have spaces between them which allow heat flow. This implies that heat can be passed in one more path than in the case with large holes. Fo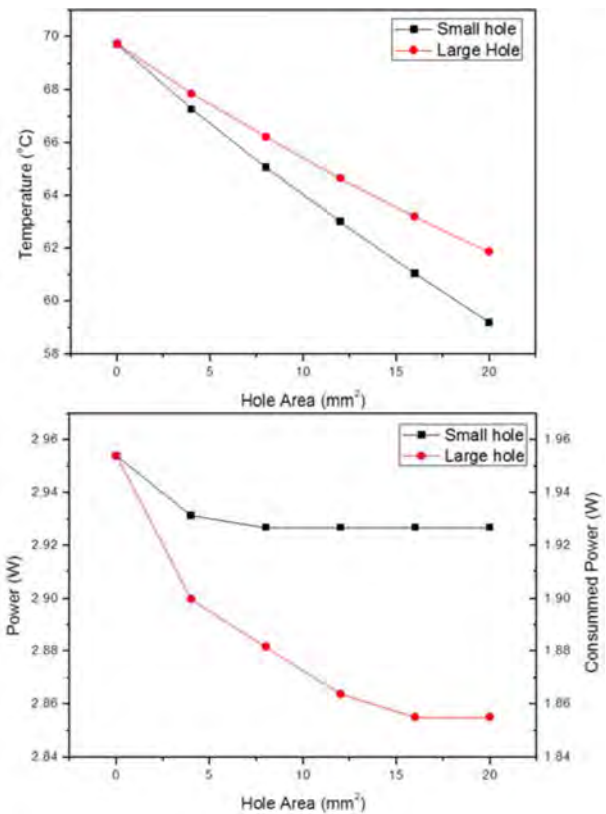r maintaining the same temperature, the sensor requires thermal isolation, which is reduced by this heat path and therefore, the substrate requires more power.

Furthermore, the cross-sectional area of the holes that are exposed to air is believed to impact the decrease in the temperature at the end of the plate. Hence, the small-hole model had lower temperature as small holes exposed a greater surface area of the substrate to air than did the large holes.
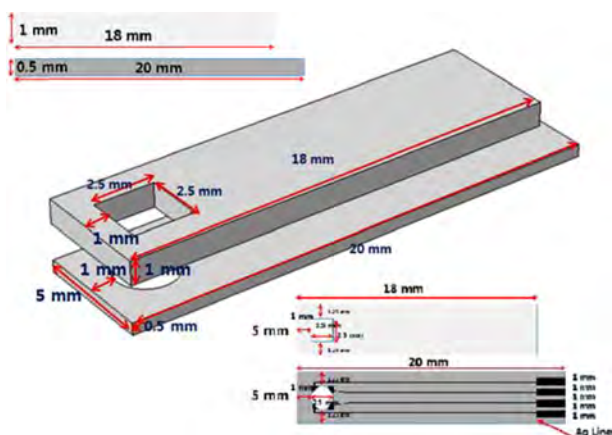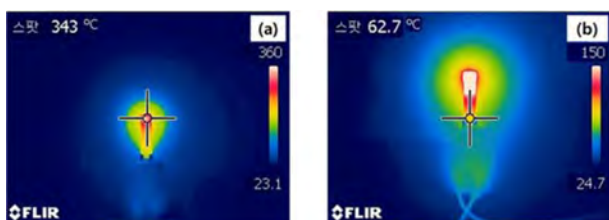
Fig. 8. Schematic structure of substrate

Fig. 9. Temperature measurement using FLIR T360 camera: (a) Temperature near the sensor operating at 6V, (b) Temperature at edge of substrate with sensor operating at 6V.

Fig. 10. Changes in temperature of substrate near sensor and edge of substrate, with respect to power.

the sensor. The temperature of the substrate near the sensor was 343°C and that at the edge-point of the substrate was 62°C. Fig. 10 shows the temperature changes in the substrate achieved by changing the power. The results indicate the possibility of heat transfer being blocked for 2 cm. Moreover, a reduction in the power consumption was expected owing to a reduction in the volume of the substrate.

4. CONCLUSIONS

A new class of self-heating gas sensors with plate structures is proposed. We conducted a comprehensive set of 3D, numerical thermal and electrical simulations for designing this new generation of substrates. The COMSOL Multiphysics simulator was used for analyzing device and circuit simulations through a direct extraction of components from the sensor.

The results revealed that a 2.035-mm circle-type model demonstrated the lowest temperature (under 65°C), at least when the total hole area was over 15 mm^2. Furthermore, the power consumed by the substrate excluding that by the sensor was found to be just 1.8 W. Our design is therefore completely compatible with mass production processes because attachment of the sensor is possible without the use of wires, thus simplifying the process. Additionally, the system was developed in chip form for PCB boards, which makes it usable in various other devices and. applicable to a four-channel sensor as well.

Finally, the practical substrate developed using LTCC demonstrated reasonable ability to be used with a high-temperature sensor directly attached to it. Therefore, this work can

3.2 Discussions of modeling and simulation

Based on these results, the substrate was designed and fabricated using the tape casting method, and its material was developed using LTCC (AMOTech). We attempted to observe how the consumed power and temperature changed in the fabricated substrate.

As shown in Fig. 8, the substrate was divided into two layers. The length, width, and depth of the bottom layer were 20, 5, and 0.5 mm, respectively. In the bottom layer, Ag paste was printed for connecting the sensor electrode and heater. The length, width, and depth of the top layer were 18, 5, and 1 mm, respectively. In the top layer, a square-type hole was punched for inserting the sensor. The contact shape was maintained as a circle of diameter 2.5 mm for both the top and bottom layers, according to the results of the simulation.

A heater with resistance of 15 Ω was embedded in the sensor and attached to the substrate hole. A heat distribution experiment was conducted by applying incremental power to the sensor by increasing the voltage from 3 to 6 V and results were confirmed using an FLIR T360 camera. Fig. 9 provides an example of the measured temperature of the substrate with 6 V power applied to
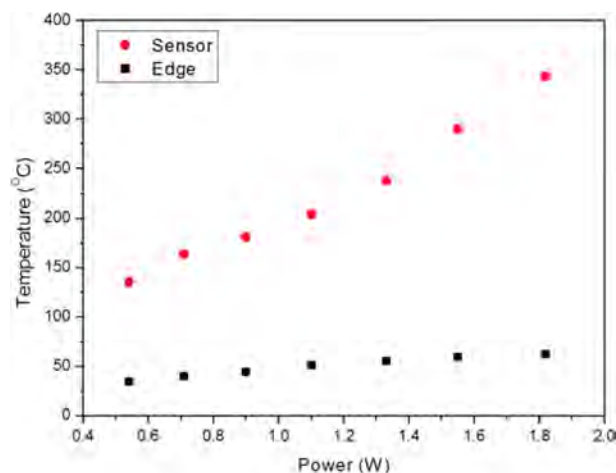
be used for designing substrates during the manufacturing of self-heated sensors. Moreover, this project is expected to be applicable for verifying the functional accuracy of sensors and their compatibility with electronic packaging with substrates during commercialization.

ACKNOWLEDGMENT

REFERENCES

[1] C. O. Park, S. A. Akbar, and W. Weppner, "Ceramic electrolytes and electrochemical sensors", *Journal of Mate-rials Science*, Vol. 38, pp. 4639-4660, 2003.

[2] C. O. Park and S. A. Akbar, "Chemical sensors for pollution monitoring and control", *Journal of Materials Science,* 38 (2003) 4237.

[3] G.S. Chung and J.M. Jeong, "Fabrication of micro heaters on polycrystalline 3C-SiC suspended membranes for gas sensors and their characteristics", *Microelectronic Engineering*, Vol. 87, pp.2348-2352, 2010.

[4] C.O Park, S.A Akbar, and J Hwang, "Selective gas detection with catalytic filter", *Materials Chemistry and Physics*, Vol. 75, pp. 56-60, 2002.